*Supplementary Information for*

# Revealing the roles of light and heat for enhanced interfacial charge transfer in photocatalytic conversion of methanol to formaldehyde coupled with hydrogen evolution

Houkui Xiang, [a, b] Wanqi Liu, [c] Zhaokai Zeng, [d] Jingxian Chen, [d] Beile Lin, [a] Guoliang Zhang, [d] Xuhui Wei, [e] Songbo Zhou, [a, b] Tongqiang Xiong, [a, b*] Pengfei Li, [c, *] and Libing Qian [d, *]

[a] School of Automation, Hubei University of Science and Technology, Xianning 437100, China

[b] Key Laboratory of Optoelectronic Sensing and Intelligent Control, Hubei University of Science and Technology, Xianning 437100, China

[c] School of Nuclear Science and Technology, Harbin Engineering University, Harbin 150001, China

[d] Hubei Key Laboratory of Radiation Chemistry and Functional Materials, School of Nuclear Technology and Chemistry & Biology, Hubei University of Science and Technology, Xianning 437100, China

[e] College of Chemistry and Chemical Engineering, Anqing Normal University, Anqing 246133, China

[*]Author to whom correspondence should be addressed: Xiongtongqiang@hbust.edu.cn; lipf2022@hrbeu.edu.cn; qianlb@hbust.edu.cn.

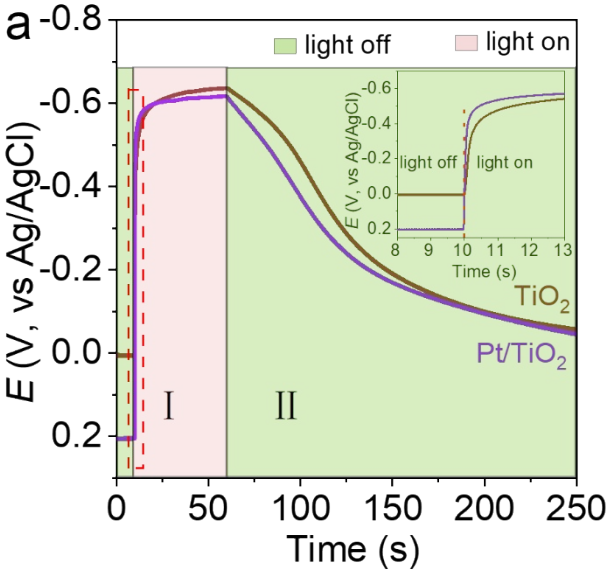


**Fig. S1** The open-circuit potential (OCP) decay behaviors of a $TiO_2$ electrode and a $Pt/TiO_2$ electrode were examined in a 15 vol% $CH_3OH$ aqueous solution. To enhance the visibility of potential changes at the semiconductor electrode, the relevant portion of the curve was locally magnified. By comparing the rates of potential change during the oxidation (region I) and reduction processes (region II), it was observed that the oxidation kinetics were significantly faster for all electrodes, occurring within a few seconds, whereas the reduction process required hundreds of seconds, even in the presence of an efficient reduction cocatalyst such as Pt.

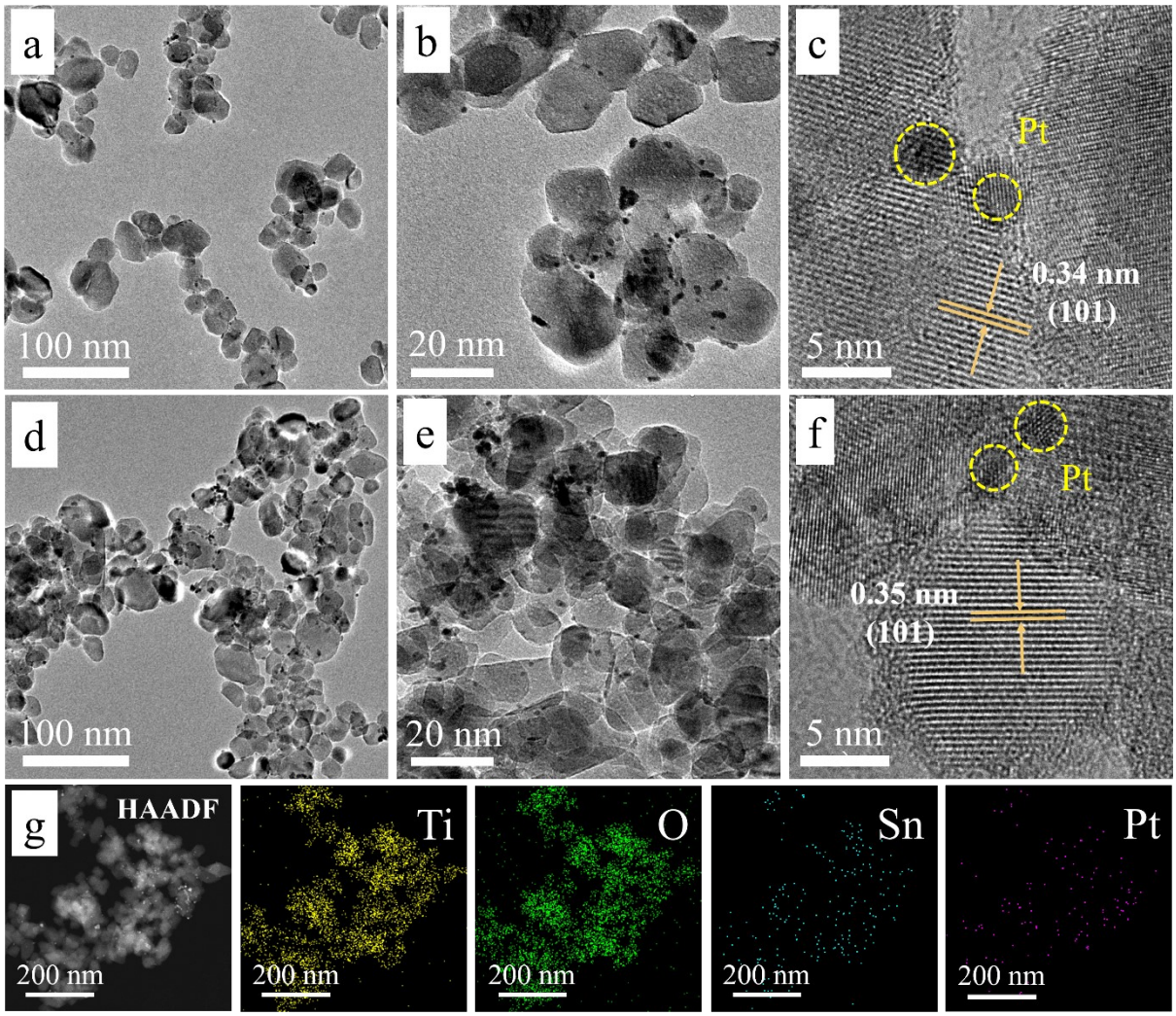


**Fig. S2** HR-TEM images of the Pt/$TiO_2$ (a, b & c) and Pt/3% Sn–$TiO_2$ (d, e & f) samples. (g) displays the HAADF image and EDX elemental mappings of the Pt/3% Sn–Pt/$TiO_2$ composite photocatalyst. Prior to the photo-deposition of platinum particles, both $TiO_2$ and 3% Sn–$TiO_2$ supports were subjected to air annealing at 500 °C for 1.5 h. The corresponding lattice fringes were observed, indicating that nanoparticles formed with good crystallinity after the annealing. The interplanar spacing was determined to be 0.34 nm for the $TiO_2$ and 0.35 nm for the 3% Sn–$TiO_2$, corresponding to the (101) crystal face in the anatase phase, since the ionic radius of $Sn^{4+}$ (69 pm) is larger than that of the lattice $Ti^{4+}$ (60.5 pm) [1, 2]. Moreover, the EDX elemental mappings confirm a uniform distribution of both the tin dopant and deposited platinum in the Pt/3 % Sn–$TiO_2$ structure.

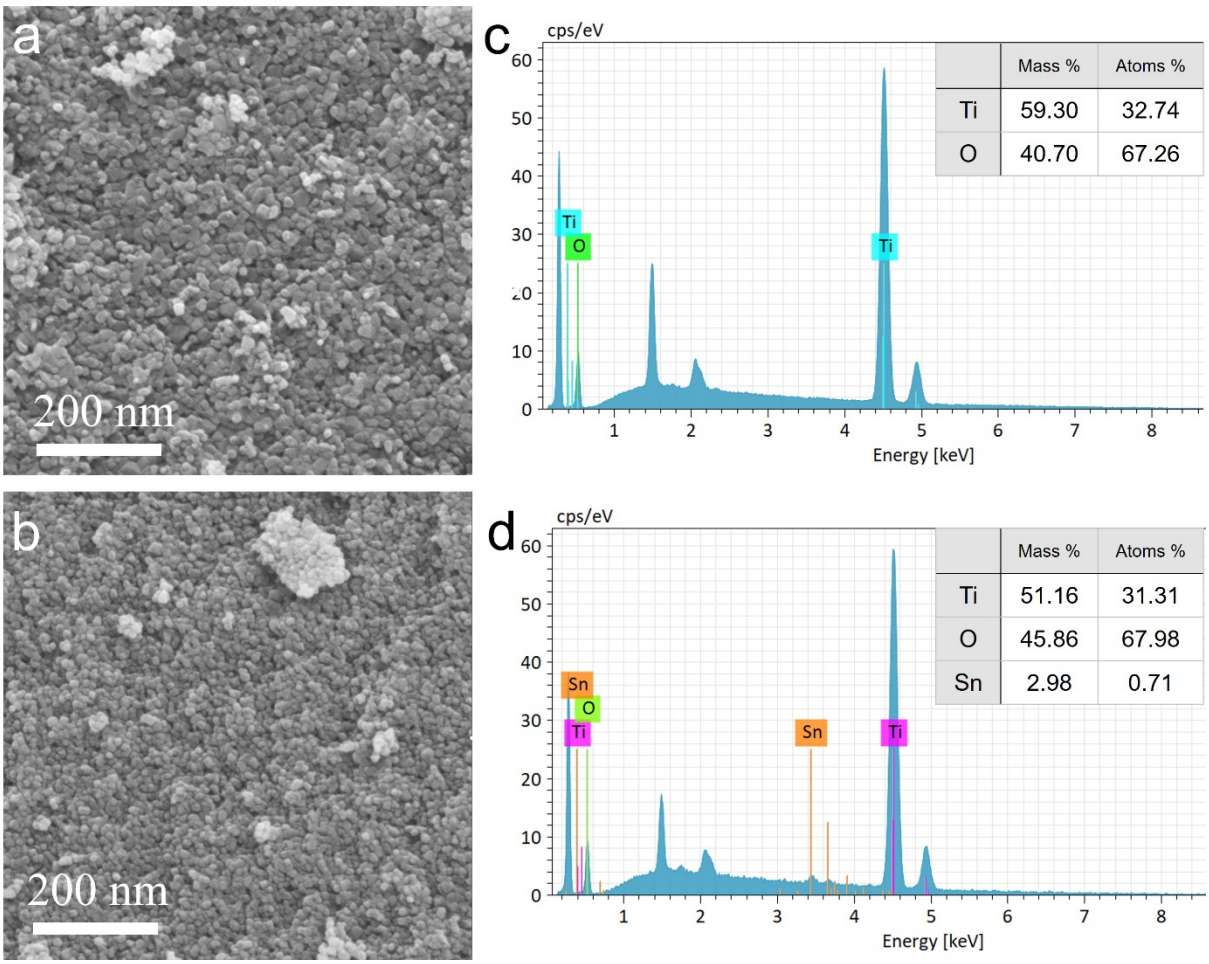


**Fig. S3** Electron microscopy images for the $TiO_2$ (a) and 3% Sn–$TiO_2$ (b). The EDX analysis (c and d) confirms the presence of Sn in the sample, validating the successful implementation of the tin doping process. However, the actual Sn content is lower than theoretically expected, possibly due to incomplete incorporation of $Sn^{4+}$ ions into the $TiO_2$ lattice during synthesis.

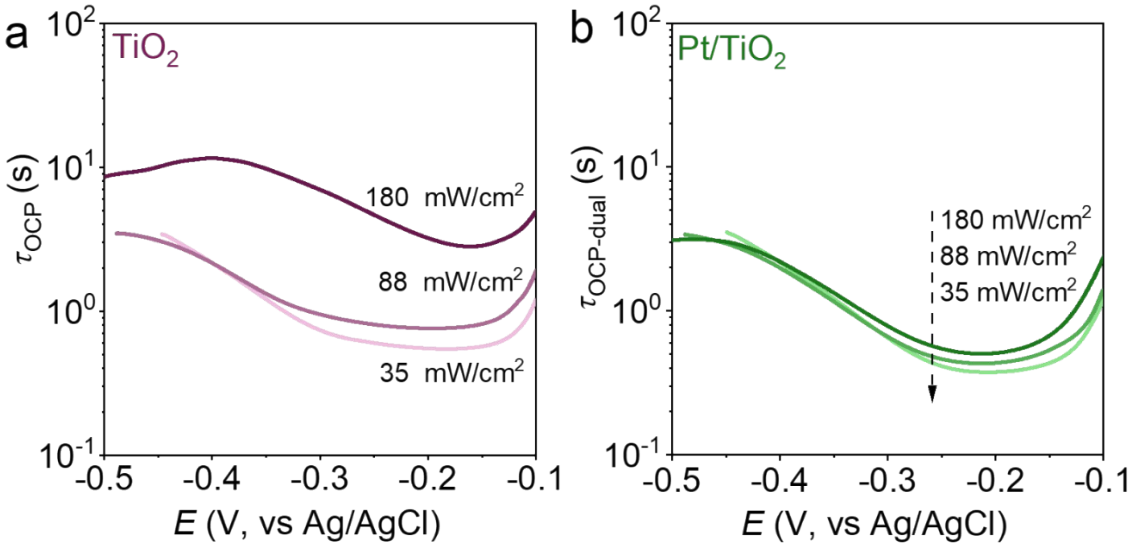


**Fig. S4** The estimated time constants of various electrodes in argon bubbled 15vol% LA aqueous solution under different irradiation intensity at the room temperature.

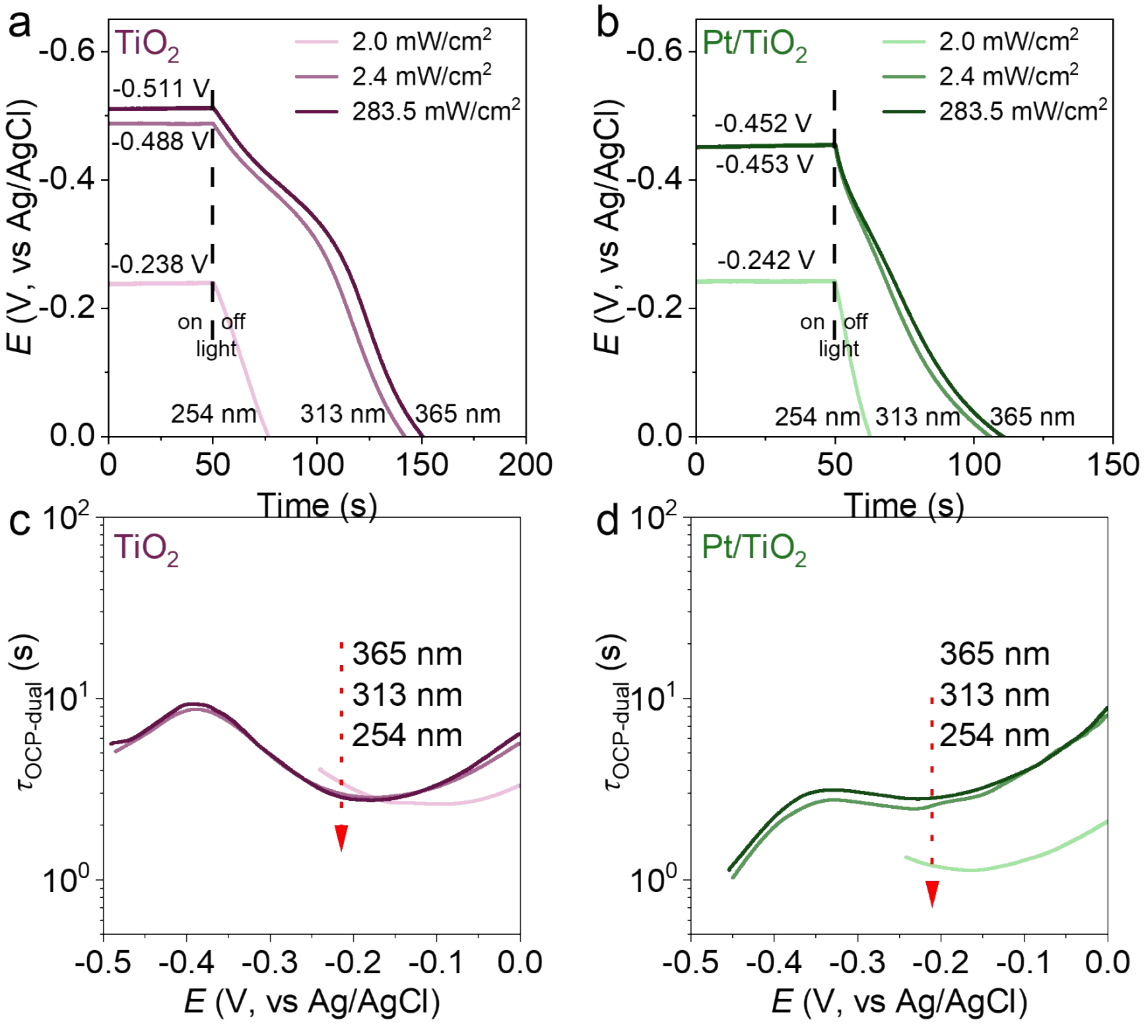


**Fig. S5** The OCP behaviors of various electrodes ($TiO_2$|FTO, Pt/$TiO_2$|FTO) were investigated in an Ar-saturated 15 vol% LA aqueous solution under different wavelength irradiation conditions at room temperature. The estimated time constants are summarized in panels (c) and (d).

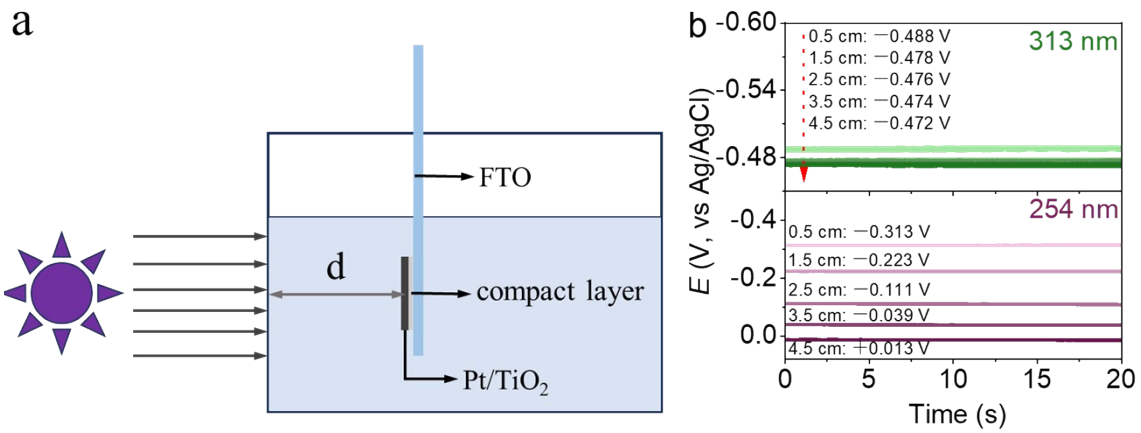


**Fig. S6** Schematic diagram (a) illustrates the device for measuring the distance-dependent photoelectrochemical behaviors (b) of $Pt/TiO_2$ electrode in an Ar-bubbled LA aqueous solution. The experimental results show that under 313 nm irradiation (~2.7 $mW/cm^2$), when the electrode spacing (d) increases from 0.5 cm to 4.5 cm, the photovoltage decreases by only 0.016 V. In contrast, under 254 nm irradiation (~2.0 $mW/cm^2$), the same increase in electrode spacing results in a photovoltage decrease of 0.326 V, approximately 20.4 times greater than that observed under 313 nm irradiation. This indicates that shorter wavelengths correspond to reduced light penetration ability in the solution. The irradiation was supplied by a Hg lamp combined with a band-pass filter. The Ag/AgCl reference electrode was shielded to prevent the shift in the reference potential.

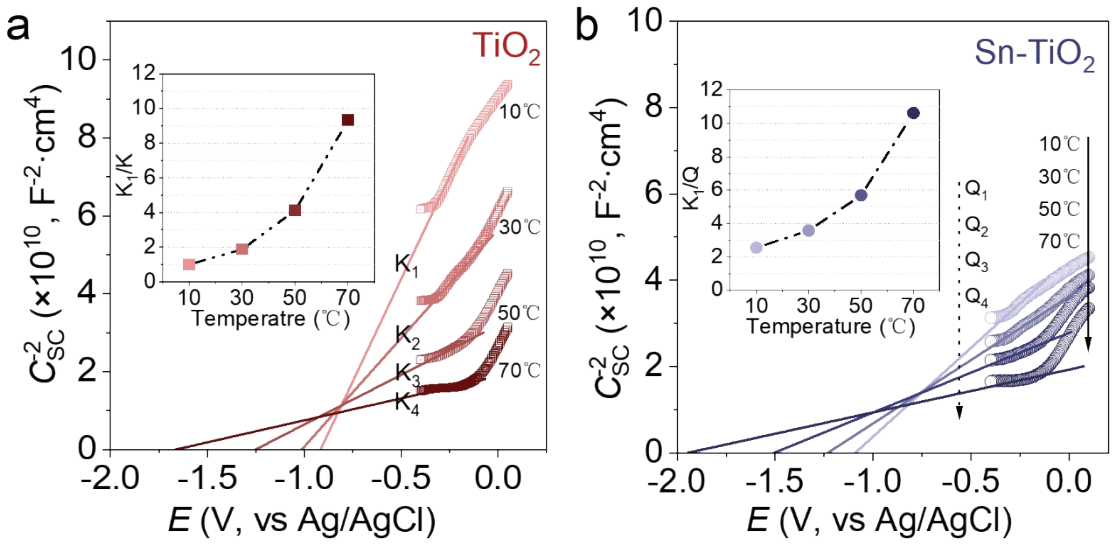


**Fig. S7** The Mott-Schottky curves of $TiO_2$ (a) and Sn–$TiO_2$ (b) electrodes in a 0.5 M $Na_2SO_4$ aqueous solution at various temperatures and a frequency of 1000 Hz are presented. The insets depict the slope ratios normalized to the slope of pure $TiO_2$ at 10 °C for other temperatures. Based on the Mott-Schottky theory, the slope is inversely proportional to the donor concentration ($N_d$). Therefore, under identical conditions, the $N_d$ of 1% Sn–$TiO_2$ at 10 °C, 30 °C, 50 °C, and 70 ℃ are 2.56, 1.90, 1.38, and 1.14 times higher than those of pure $TiO_2$, respectively. This indicates that Sn doping effectively enhances the donor concentration. Additionally, for pure $TiO_2$, the $N_d$ increases by 9.33 times as the temperature rises from 10 °C to 70 °C. In contrast, for Sn–$TiO_2$, the donor concentration only increases by 4.16 times within the same temperature range. These findings reveal that Sn doping can mitigate charge leakage induced by temperature elevation, which is essential for achieving efficient photothermal catalysis under high light intensity.

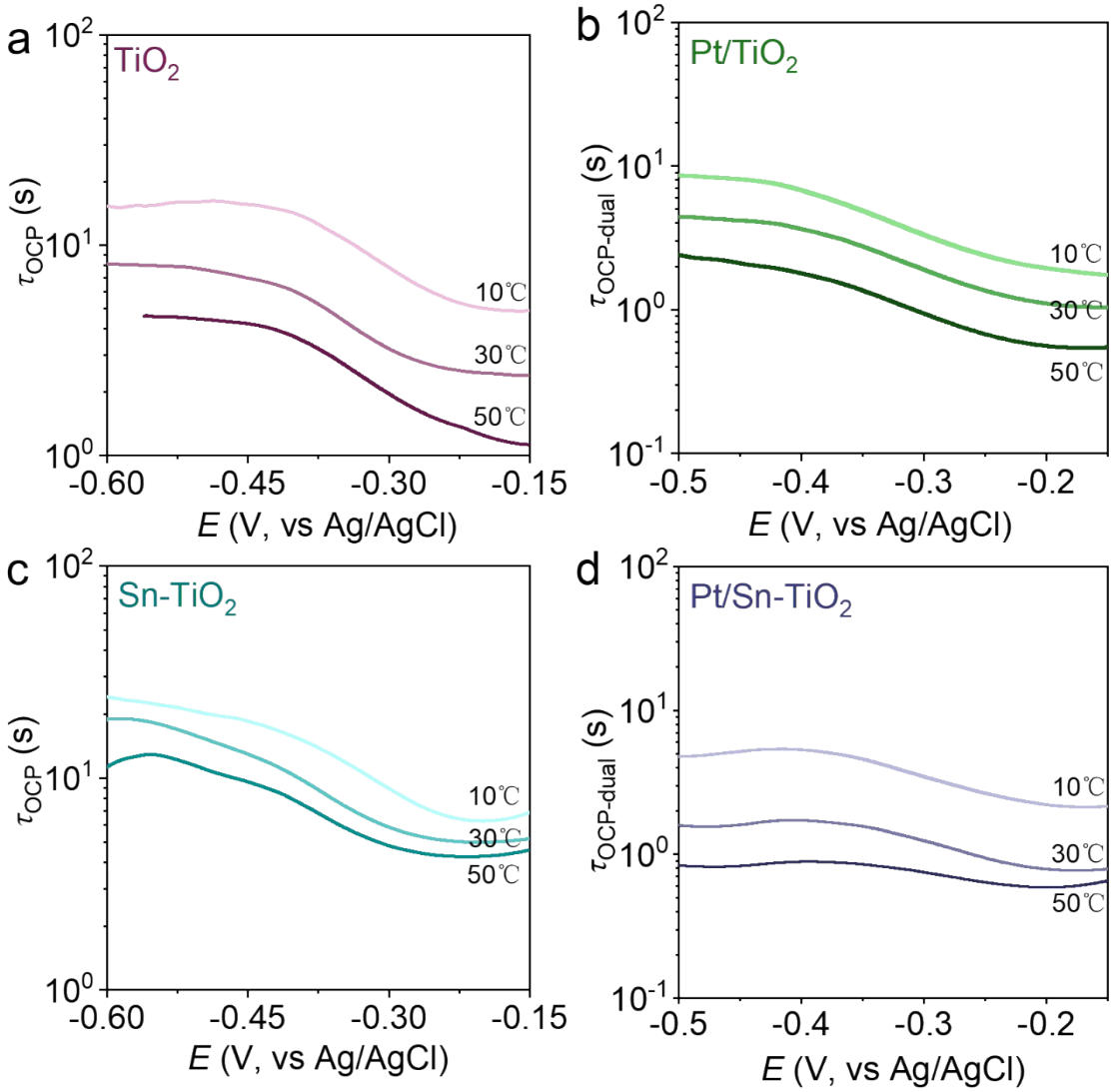


**Fig. S8** The estimated time constants of various electrodes in argon bubbled 15 vol% LA aqueous solution under identical UV lamp irradiation at different temperatures.

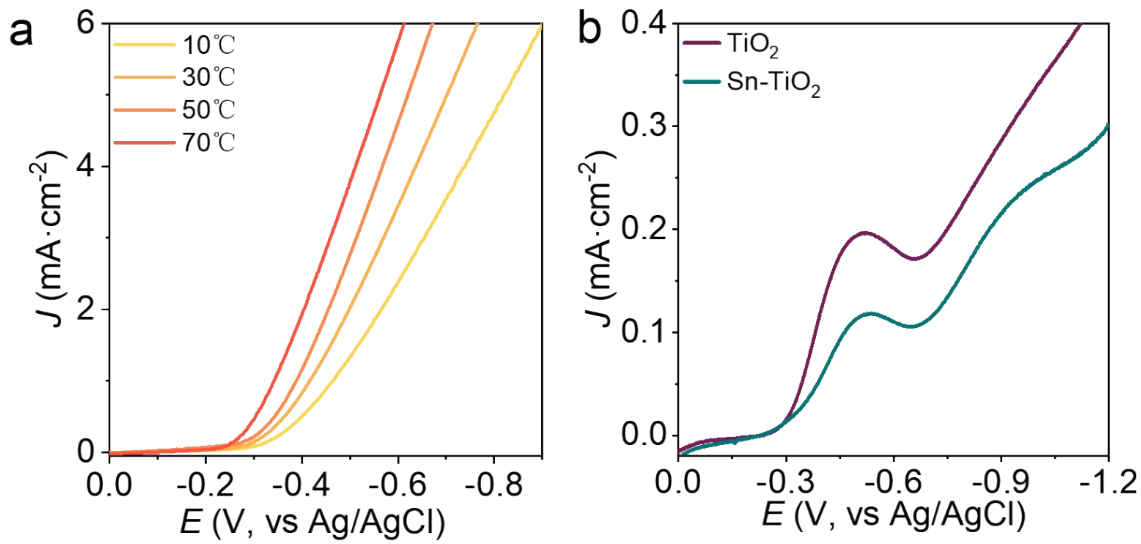


**Fig. S9** Linear Sweep Voltammetry (LSV) curves of a Pt electrode in an argon-bubbled 0.5 M $H_2SO_4$ solution at varied temperatures (a). The onset potential for the hydrogen evolution reaction (HER) shifts positively with increasing temperature, indicating enhanced HER kinetics under elevated thermal conditions. Rotating disk electrode (RDE) voltammograms (1600 rpm) comparing the oxygen reduction reaction (ORR) activity of $TiO_2$ and 1% Sn–$TiO_2$ modified electrodes in an oxygen-bubbled 0.1 M KOH (b). 1% Sn–$TiO_2$ exhibits a more negative ORR onset potential compared to pure $TiO_2$, suggesting less efficient electron transfer to oxygen molecules and indicating that Sn doping introduces an additional kinetic barrier for the ORR.

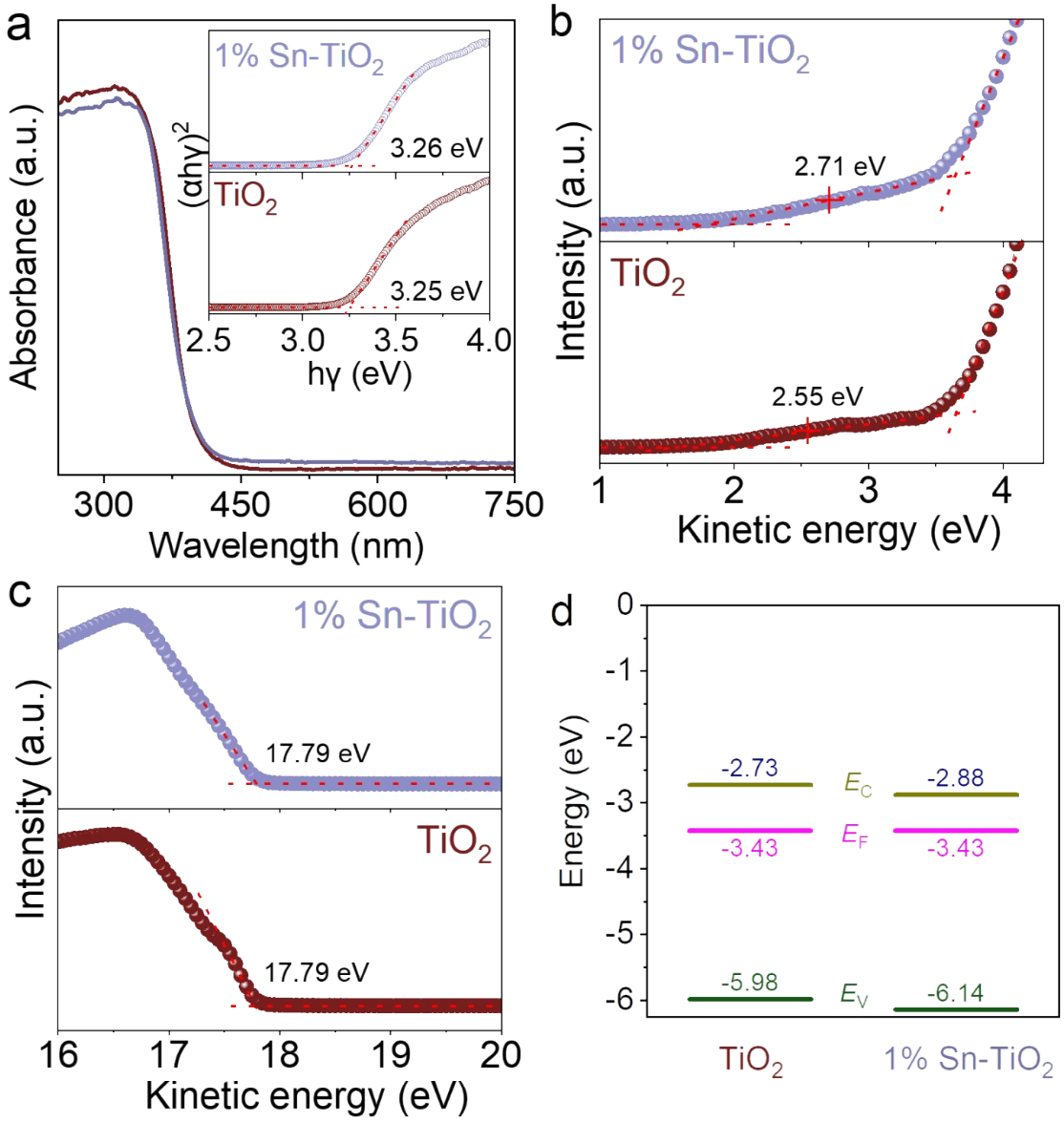


**Fig. S10** The UV-vis absorption spectra of $TiO_2$ and 1% Sn–doped $TiO_2$ (a), together with the UPS test results obtained under a bias voltage of −5 V (b and c), were comprehensively analyzed. Based on the data, the valence band region (c) and secondary electron cutoff energy (d), along with the energy band structure diagrams were constructed (d). The analysis reveals that the band gap remains nearly unchanged after doping with 1% Sn, while the conduction band position decreases by 0.15 eV. This suggests a significant reduction in the SC barrier, which facilitates interfacial electron transfer.

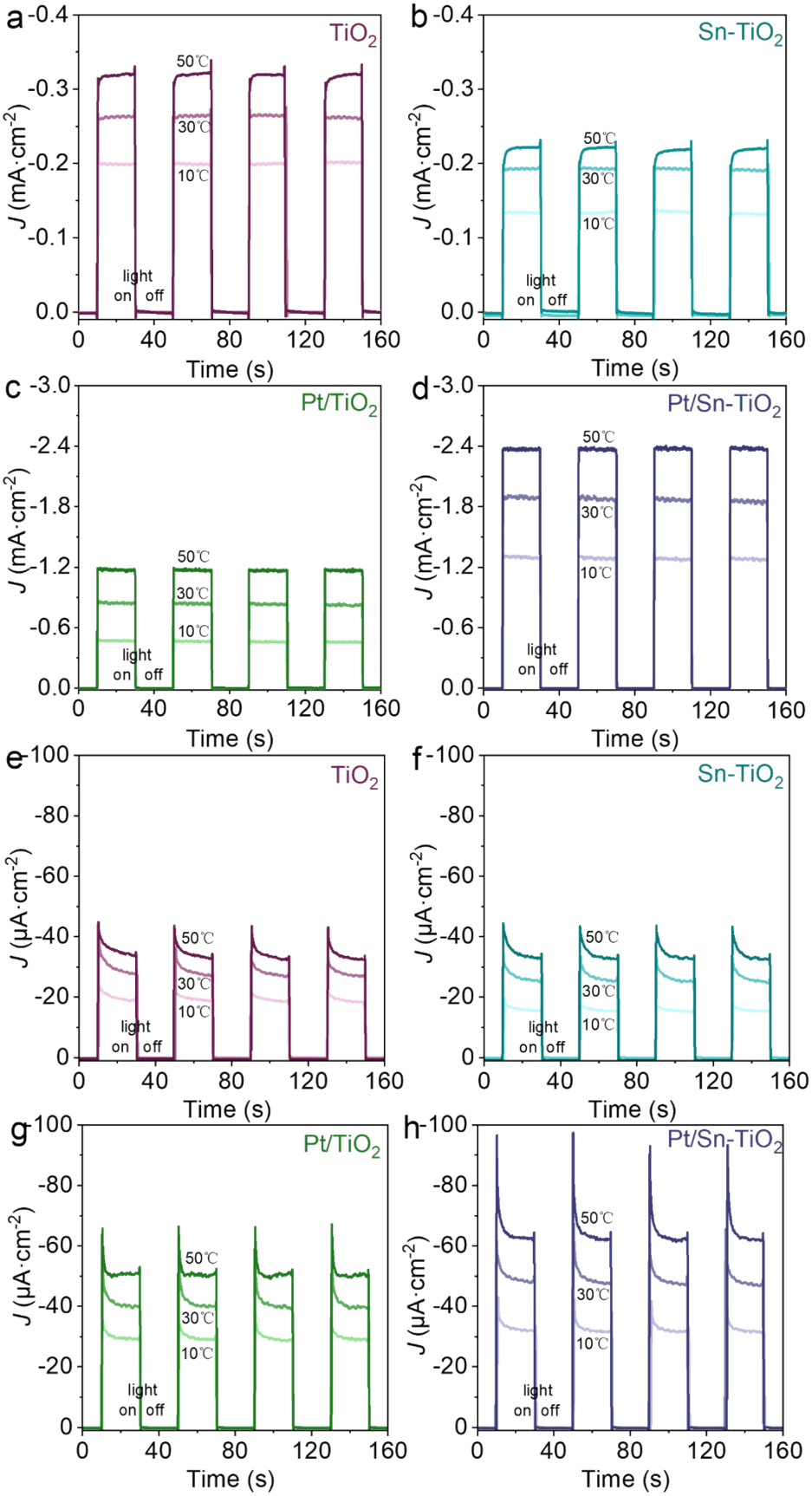


**Fig. S11** Photoinduced the anodic behaviors of electrodes ($TiO_2$|FTO, Sn–$TiO_2$|FTO, Pt/$TiO_2$|FTO, and Pt/Sn–$TiO_2$|FTO) in argon bubbled 15 vol% LA aqueous (a-d) and 0.5 M $Na_2SO_4$ aqueous solution (e-h) at various temperature.

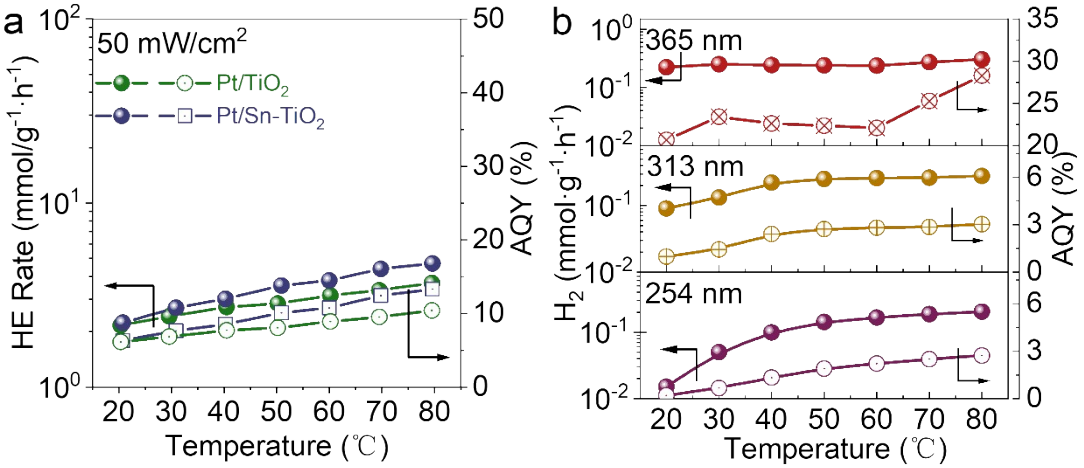


**Fig. S12** Photothermal catalytic HE rates and AQY of $Pt/TiO_2$ and $Pt/Sn–TiO_2$ in a 15 vol% LA aqueous solution under 50 mW/cm$^2$ (AM 1.5G) irradiation (with an effective photon flux of $1.18 \times 10^{17}$ photons·s$^{-1}$) (a). Panel (b) shows the temperature-dependent HE performance of $Pt/TiO_2$ in 15 vol% LA aqueous solution under irradiation at 254 nm (~1.7 mW/cm$^2$), 313 nm (~2.0 mW/cm$^2$), and 365 nm (~100 mW/cm$^2$). The $H_2$ production rates are normalized to incident light intensity (per mW/cm$^2$) to facilitate comparison across different experimental conditions.

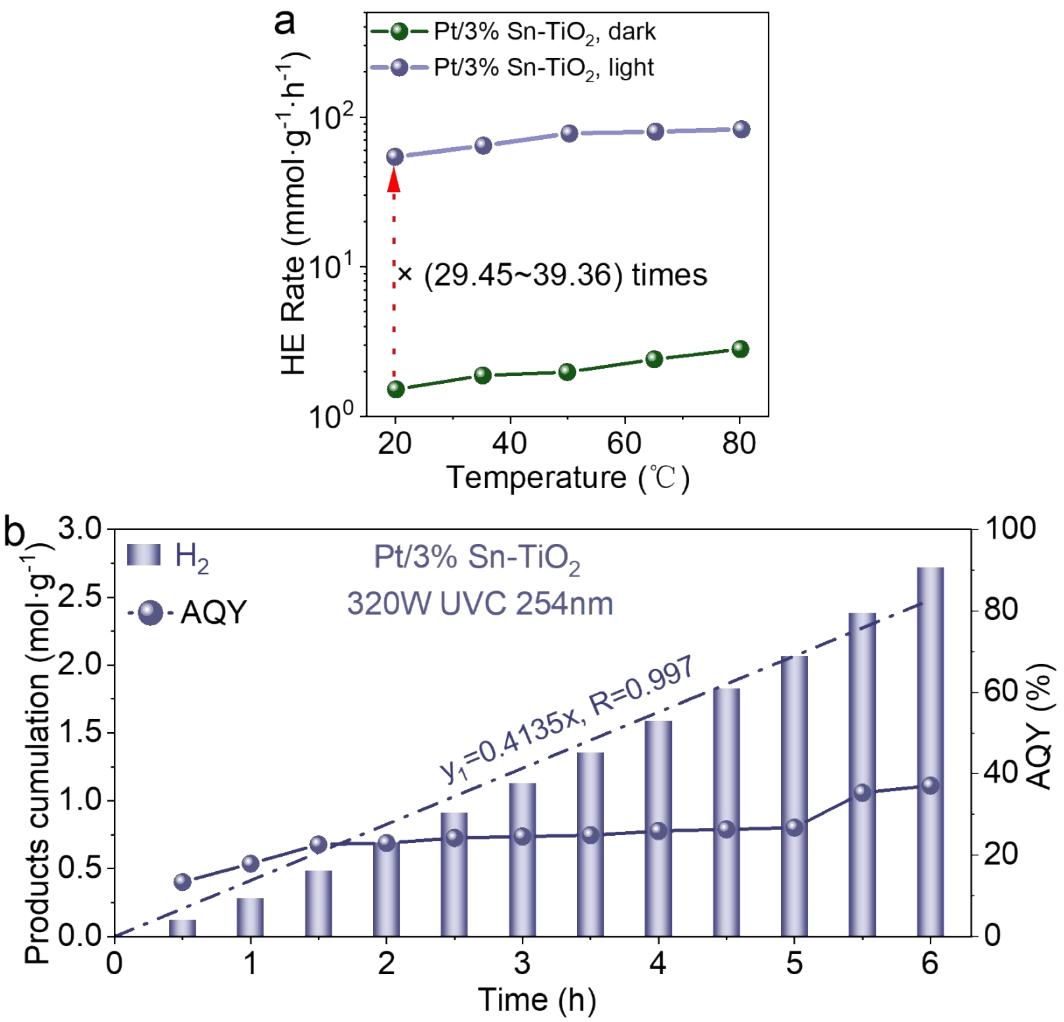


**Fig. S13** Photothermal catalytic HE performance of Pt/3% Sn–$TiO_2$ in 15 vol% $CH_3OH$ aqueous solution under the light (30 W, 254 nm) irradiation, dark conditions (a), and 320 W UV irradiation (b) (Reaction conditions: Ar-bubbled in 1000 ml 20 vol% $CH_3OH$ aqueous solution, 320 W low-pressure mercury lamp (254 nm)). Over a 6 h reaction at 80 °C, the average $H_2$ production rate reached as high as 413.5 mmol·$g^{-1}$·$h^{-1}$, with an AQY of 25.16%.

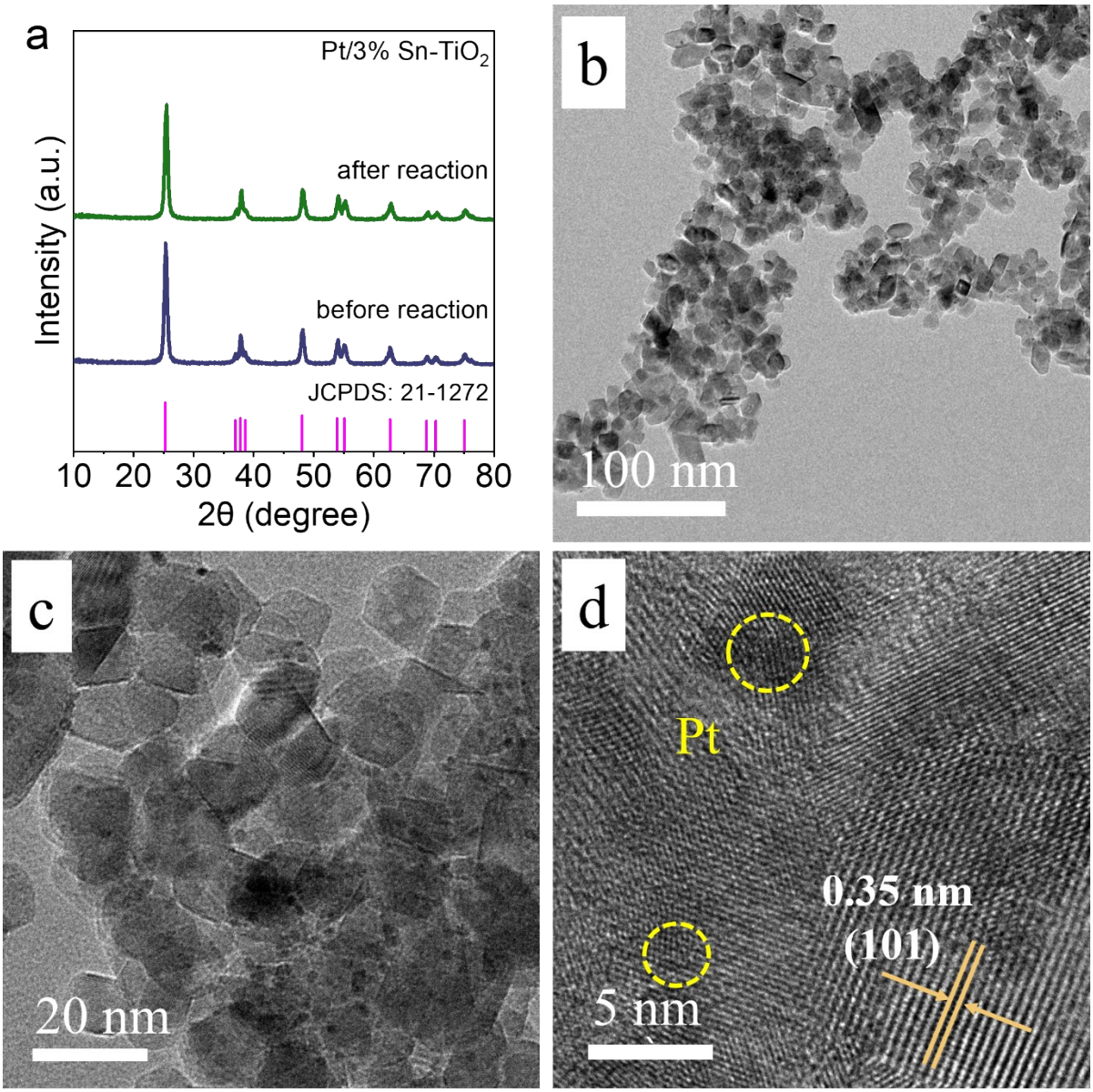


**Fig. S14** The XRD patterns (a) and HR-TEM images (b-d) of the Pt/3% Sn–$TiO_2$ catalyst after 12 h of photocatalytic $CH_3OH$ conversion are presented. A comparison of the structural and morphological characteristics before and after (Fig. S2d-S2f) the reaction reveals no significant changes in either crystal phase or microstructure, confirming the excellent structural stability of the catalyst under the employed reaction conditions.

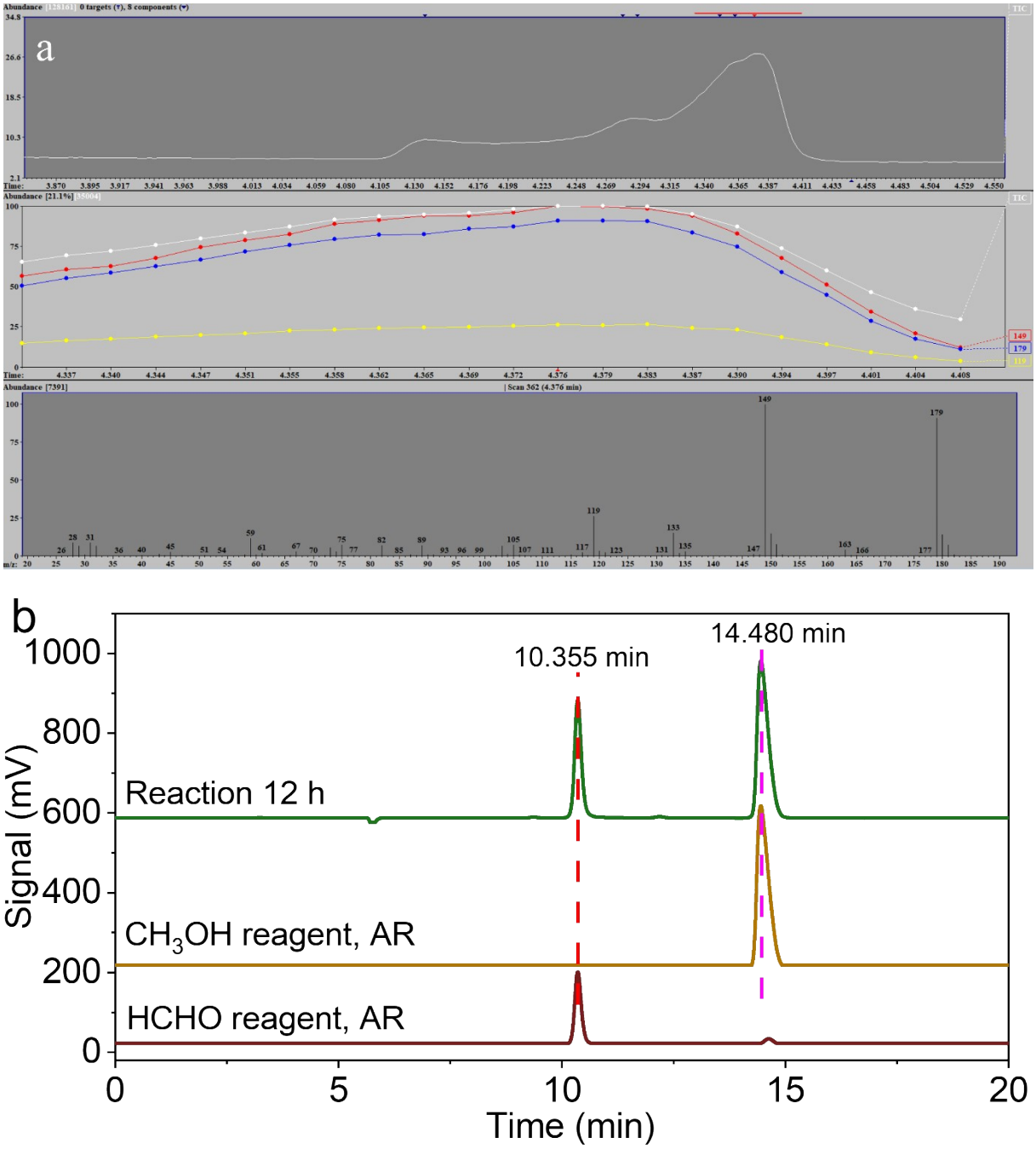


**Fig. S15** The GC–MS (a) and HPLC (b) analyses of a 20 vol% $CH_3OH$ aqueous solution after 12 h of reaction. For comparison, HPLC analysis was also carried out on the original 20 vol% $CH_3OH$ aqueous solution (AR) used as the reactant, as well as on a commercial HCHO reagent (AR, diluted with deionized water to meet detection requirements) (b). As reported in the literature,[3, 4] free HCHO molecules in aqueous solutions are present at very low concentrations and readily undergo polycondensation. Accordingly, the HCHO ion peak at *m/z* 29 is not clearly discernible in the mass spectrum. In contrast, prominent fragment ion peaks are observed at *m/z* 89, 119, 149, and 179, which correspond to characteristic fragments of oligomeric formaldehyde.[5, 6] Additional ion peaks detected at *m/z* 45 and 59 are tentatively assigned to formic acid and methyl formate, respectively.[7] Notably, the HPLC results (b) clearly confirm the presence of HCHO in the liquid product after 12 h of reaction, indicating its formation via the photocatalytic process.

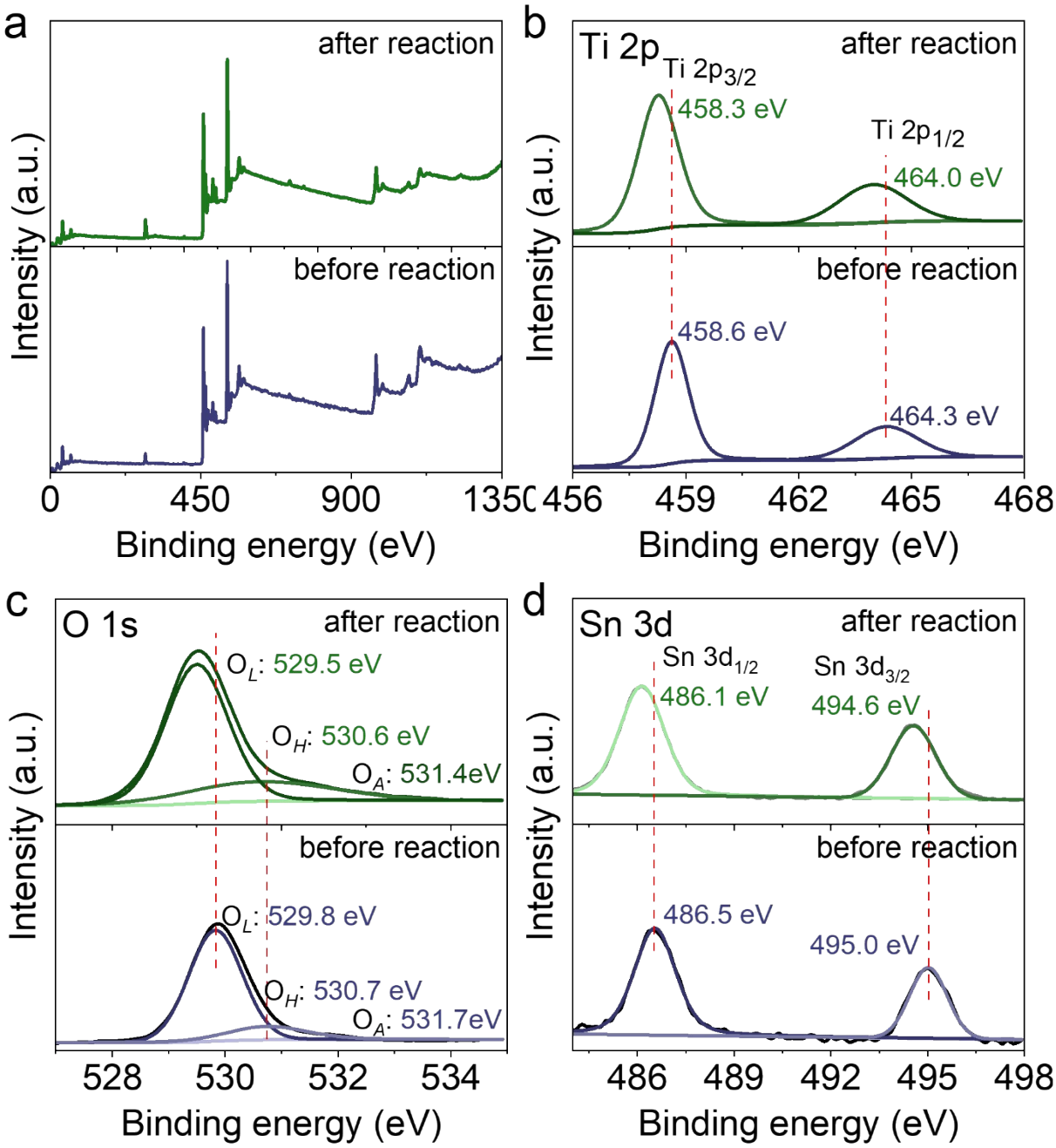


**Fig. S16.** XPS spectra of the catalyst before and after the reaction are presented in panel (a), along with high-resolution scans of the Ti 2p (b), O 1s (c), and Sn 3d (d) regions. Comparative analysis reveals a consistent shift toward lower binding energies in the Ti 2p, O 1s, and Sn 3d core-level spectra after 12 h of catalytic reaction, which aligns with previously reported phenomena.[8, 9] This shift can be attributed to the considerably higher rate of the oxidation half-reaction relative to that of the reduction half-reaction during the catalytic process. Such kinetic imbalance disturbs the equilibrium between charge separation and extraction, leading to substantial accumulation of electrons on the catalyst surface. As a result, partial reduction of $Ti^{4+}$ and $Sn^{4+}$ to lower-valent states (e.g., $Ti^{3+}$ and $Sn^{2+}$) is promoted. The increased electron density at these metal centers reduces the core-level binding energies, thereby inducing the observed shift in the XPS spectra.

**Tab. S1** Comparison of photocatalytic oxidation of $CH_3OH$ into HCHO and $H_2$ over various photocatalysts reported in recent reports.

| Photocatalyst | Reaction conditions | $H_2$ ($mmol \cdot g^{-1} \cdot h^{-1}$) | HCHO ($mmol \cdot g^{-1} \cdot h^{-1}$) | Ref. |
|---|---|---|---|---|
| CuS | light: 300 W Xe lamp (780 nm > λ > 420 nm); reactants: 5 mL 76 wt% $CH_3OH$ aqueous solution, $N_2$ | 0.11 | 0.13 | 10 |
| $Cu/TiO_{2-x}/CoP$ | light: 350 W Xe lamp (λ≥ 420 nm); reactants: 100 mL 20 vol% methanol aqueous solution | 0.378 | / | 11 |
| g-$C_3N_4$ | light: 300 W Xe lamp (780 nm > λ > 320 nm); reactants: 5 mL 76 wt% $CH_3OH$ aqueous solution, $N_2$ | 1.5 | 0.79 | 10 |
| Au8@m$TiO_2$ | light: 150 W Halogen lamp (λ > 360 nm, 100 $mW/cm^2$); reactants: 4 mL $CH_3OH$; | 1.503 | / | 12 |
| $TiO_2$ | light: 300 W Xe lamp (780 nm > λ > 320 nm); reactants: 5 mL 76 wt% $CH_3OH$ aqueous solution, $N_2$ | 2.0 | 1.6 | 10 |
| 2D-2D 0.5 wt% $MoS_2/TiO_2$ | light: 300 W Xe lamp; reactants: 100 mL 10 vol% $CH_3OH$ aqueous solution, 20 ℃ | 2.145 | / | 13 |
| $OPCS_V$-15 | light: 500 W Xe lamp (λ > 420 nm); reactants: 5 mL 2.5 M $CH_3OH$ alkaline (1.0 M NaOH) aqueous solution, $P_{O_2}$: 1 atm, 25 ℃ | 2.321 | / | 14 |
| ZnO | light: 300 W Xe lamp (780 nm > λ > 320 nm); reactants: 5 mL 76 wt% $CH_3OH$ aqueous solution, $N_2$ | 3.1 | 3.0 | 10 |
| $N_{V_N}$-g-$C_3N_4$ | light: 300 W Xe lamp (λ > 420 nm); reactants: 25 vol% $CH_3OH$ aqueous solution | 3.17 | / | 15 |
| ZnS | light: 300 W Xe lamp (780 nm > λ > 320 nm); reactants: 5 mL 76 wt% $CH_3OH$ aqueous solution, $N_2$ | 3.4 | 2.2 | 10 |
| $Cu_{2-x}S/CdS/Bi_2S_3$ | light: 300 W Xe lamp (λ > 420 nm); reactants: 100 mL 20 vol% $CH_3OH$ aqueous solution | 8.012 | / | 16 |
| 5 wt% $MoS_2$ foam/CdS nanorod | light: 300 W Xe lamp (780 nm > λ > 420 nm); reactants: 5 mL 76 wt% $CH_3OH$ aqueous solution, $N_2$ | 12 | 2.5 | 10 |
| MgO | light: 1000 W mercury lamp (2500 nm > λ > 200 nm); reactants: 8 mL$CH_3OH$ solution, air, 25℃ - 37 ℃ | 0.32 | / | 17 |
| $Fe/CeO_2$ | light: 125 W middle-pressure mercury lamp (λ ≥ 400 nm); reactants: 50 mL 10 vol% $CH_3OH$ aqueous solution, Ar | 12.82 | / | 18 |
| SCN 550 | light: 300 W Xe lamp; reactants: 40 mL 50 vol% $CH_3OH$ aqueous solution, pH = 12, 90 ℃ | 14.7 | / | 19 |
| Pt/g-$C_3N_4$ porous nanosheet | light: 300 W Xe lamp; reactants: 30 mL 50 vol% $CH_3OH$ aqueous solution | 17.12 | / | 20 |
| Cu 50/$TiO_2$ nanosheets | light: 300 W Xe lamp; reactants: 50 mL $CH_3OH$ solution, Ar, 25 ℃ | 17.8 | / | 21 |
| 1% Cu/PC50 | light: 300 W Xe lamp; reactants: 20 mL 50 vol% $CH_3OH$ aqueous solution, 60 ℃ | 33.702 | / | 22 |
| 3 wt% Pt@CN | light: 300 W Xe lamp; reactants: 80 mL 25 vol% $CH_3OH$ alkaline aqueous solution (pH = 12), Ar, 35 ℃ | 35.6 | / | 23 |
| Ni/CdS | light: 300 W Xe lamp (λ > 420 nm); reactants: 5 mL $CH_3OH$ solution, Ar, 20 ℃ | 48.2 | / | 24 |
| $Co/Cd_{0.5}Zn_{0.5}S$ | light: 300 W Xe lamp (780 nm > λ > 350 nm); reactants: 100 mL 4 vol% $CH_3OH$ alkaline | 178.4 | / | 25 |

| | | | | |
|---|---|---|---|---|
| | aqueous solution (NaOH: 4 M), Ar, 60 ℃ | | | |
| $Ni_3Sn_1/Al_2O_3$ | light: 500 W high-pressure mercury lamp; reactants: 10 mL 25 vol% $CH_3OH$ aqueous solution, Ar, 2 atm, 150 ℃ | 16.626 | / | 26 |
| 6 wt% Ni/ZIS NCs | light: 30 W UV lamp (λ = 365 nm); reactants: 5 mL 80% $CH_3OH$ aqueous solution, Ar, 20 ℃ | ~65.0 | 70.4 | 27 |
| Pt@TS-1(Ti) | light: 500 W mercury lamp; reactants: 30 mL $CH_3OH$ solution, Ar, 60 ℃ | 112.7 | / | 28 |
| 1 wt% $Pt/TiO_2$ | light: 30 W low-pressure mercury lamp (λ = 254 nm); reactants: $CH_3OH$ benzenesulfonate acid solution, Ar, 55 ℃ | 207 | 195 | 29 |
| Pt/3% Sn-$TiO_2$ | light: 320 W UV lamp (254 nm); reactants: 1000 mL 20 vol% $CH_3OH$ aqueous solution, Ar, 80℃ | 413.5 | / | This work |

## Supplementary Material Reference


1. F. Lu, K. Chen, Q. Feng, H. Cai, D. Ma, D. Wang, X. Li, C. Zuo and S. Wang, *Journal of Environmental Chemical Engineering*, 2021, **9**, 105840.
2. Q. Liu, Y. Yang, Y. Ni, Q. Wang, H. Yu, X. Zhu, Z. Ying and Y. Song, *Appl. Surf. Sci.*, 2021, **570**, 151175.
3. S. K. Gupta and A. Kumar, in *Reaction Engineering of Step Growth Polymerization*, eds. S. K. Gupta and A. Kumar, Springer US, Boston, MA, 1987.
4. J. F. Walker, *Formaldehyde (Third Edition)*, Robert E. Krieger Publishing CO., INC., New York, 1975.
5. Z. Li, Z. Zhang, B. D. Kay and Z. Dohnálek, *The Journal of Physical Chemistry C*, 2011, **115**, 9692-9700.
6. J. Kim, B. D. Kay and Z. Dohnálek, *The Journal of Physical Chemistry C*, 2010, **114**, 17017-17022.
7. K. R. Phillips, S. C. Jensen, M. Baron, S.-C. Li and C. M. Friend, *Journal of the American Chemical Society*, 2013, **135**, 574-577.
8. P. Krishnan, M. Liu, P. A. Itty, Z. Liu, V. Rheinheimer, M.-H. Zhang, P. J. M. Monteiro and L. E. Yu, *Scientific Reports*, 2017, **7**, 43298.
9. D.-S. Lee and Y.-W. Chen, *Journal of Catalysts*, 2013, **2013**, 1-9.
10. S. Xie, Z. Shen, J. Deng, P. Guo, Q. Zhang, H. Zhang, C. Ma, Z. Jiang, J. Cheng, D. Deng and Y. Wang, *Nature Communications*, 2018, **9**, 1181.
11. Y. Xiao, K. Wang, Z. Yang, Z. Xing, Z. Li, K. Pan and W. Zhou, *Journal of Hazardous materials*, 2021, **414**, 125487.

12. B. Liu, M. Louis, L. Jin, G. Li and J. He, *Chemistry – A European Journal*, 2018, **24**, 9651-9657.
13. Y.-J. Yuan, Z.-J. Ye, H.-W. Lu, B. Hu, Y.-H. Li, D.-Q. Chen, J.-S. Zhong, Z.-T. Yu and Z.-G. Zou, *ACS Catalysis*, 2016, **6**, 532-541.
14. N. Lu, X. Yan, B. Wu, H. Kobayashi and R. Li, *Applied Catalysis B: Environment and Energy*, 2025, **360**, 124536.
15. R. Wang, X. Wang, X. Li, L. Pei, X. Gu and Z. Zheng, *International Journal of Hydrogen Energy*, 2021, **46**, 197-208.
16. M. Guo, T. Zhao, Z. Xing, Y. Qiu, K. Pan, Z. Li, S. Yang and W. Zhou, *ACS Applied Materials & Interfaces*, 2020, **12**, 40328-40338.
17. Z. Liu, Z. Yin, C. Cox, M. Bosman, X. Qian, N. Li, H. Zhao, Y. Du, J. Li and D. G. Nocera, *Science Advances*, **2**, e1501425.
18. S. Mansingh, D. K. Padhi and K. M. Parida, *International Journal of Hydrogen Energy*, 2016, **41**, 14133-14146.
19. H. Wang, M. Thangamuthu, Z. Wu, J. Yang, H. Yuan, M. K. Bayazit and J. Tang, *Chemical Engineering Journal*, 2022, **445**, 136790.
20. Y.-F. Liang, J.-R. Lu, S.-K. Tian, W.-Q. Cui and L. Liu, *Chinese Journal of Chemical Engineering*, 2024, **66**, 40-50.
21. F. Yu, L. Chen, X. Li, X. Shen, H. Zhao, C. Duan and Q. Chen, *ACS Applied Materials & Interfaces*, 2021, **13**, 18619-18626.
22. H. Jiao, J. Yang, X. Li, C. Wang and J. Tang, *Green Chemistry*, 2022, **24**, 8345-8354.
23. B. Wu, B. Jiang, C. Guo, J. Zhang, Q. Li, N. Wang, Z. Song, C. Tian, M. Antonietti and H. Fu, *Angewandte Chemie International Edition*, 2024, **64**, e202418677.
24. H. Huang, Y. Jin, Z. Chai, X. Gu, Y. Liang, Q. Li, H. Liu, H. Jiang and D. Xu, *Applied Catalysis B: Environmental*, 2019, **257**, 117869.
25. W. Xue, J. Tian, X. Hu, J. Fan, T. Sun and E. Liu, *Chemical Engineering Journal*, 2022, **443**, 136427.
26. R. Wang, M. Lv, J. Zhang, F. Wang, X. Wang, N. Wang, G. Yu and Z. Zheng, *Chemical Engineering Journal*, 2024, **502**, 157981.
27. J. Luo, C. Zhu, J. Li, J. Jin, N. E. Soland, P. W. Smith, Y. Shan, A. M. Oddo, A. L. Maulana, L. Jayasinghe, X. Chen, T. Wang, J.-A. Lin, E. Lu, B. Schaefer, M. Schmalzbauer, R. Zhang,

F. Seeler, C. Lizandara-Pueyo, J. Guo and P. Yang, *Journal of the American Chemical Society*, 2025, **147**, 3428-3437.

28. S. Tian, H. Guo, Q. Zhao, L. Liu, H. Wang, X. Wang, S. Zhang and W. Cui, *Applied Catalysis B: Environment and Energy*, 2024, **355**, 124201.

29. K. Jia, X. Wei, Y. Xu, Z. Wang and J. Chen, *Applied Catalysis A: General*, 2023, **650**, 119009.